

Xin-Gang Zhao^a, Zhi Wang^{a,b}, Oleksandr I. Malyi^a, Alex Zunger^{a,*}

^aDepartment of Materials Science and Engineering, National Institute of Standards and Technology, Gaithersburg, Maryland 20899, USA; ^bDepartment of Chemistry, Beijing University of Aeronautics and Astronautics, Beijing, 100083, China

Ternary ABX_3 perovskites made of corner-sharing BX_6 octahedra have long featured prominent in solid-state chemistry and condensed matter physics. Still, the joint understanding of their two main groups—*halides and oxides*—has not been fully developed. Indeed, unlike the case in simpler compounds having a single, robust repeated motif (“monomorphous”), certain bicubic perovskites can manifest a non-herminal (= intrinsic) distortion of local motifs (“polymorphous work”). Such a distortion can include positional degree of freedom (e.g., atomic displacement and octahedral tilting) or magnetic moment degree of freedom in paramagnets. Unlike hermal motifs, such a distortion does not time-average out, being an expression of the intrinsic symmetry-breaking preference of the chemical bonding. The present study compares electronic structure features of oxide and halide perovskites arising from the a priori polymorphic distortion of motifs described by Density Functional Theory (DFT) minimization of the internal energy, containing a finite temperature hermal disorder modeled via finite temperature DFT molecular dynamics. We find that (i) different *oxide vs. halide* ABX_3 compounds adopt different energy-lowering symmetry-breaking modes. The calculated pair distortion function (PDF) of $SrTiO_3$ from the first-principle agrees with recent measured PDF. (ii) In both oxide and halide, such a distortion leads to band gap *blueshifts* in the respective ordered cubic $Pm-3m$ structure. (iii) For oxide perovskites, high-temperature molecular dynamics simulation initiated from the a priori distorted polymorph structure reveals that the

Introduction

ABX_3 halide $A^{(I)}B^{(IV)}X_3^{(VI)}$ and oxide ABO_3 perovskite often crystallize as corner-sharing low-symmetry (e.g., orthorhombic or tetragonal) phases at low temperatures (LT), sometimes transforming at higher temperatures into the cubic phase. They are generally discussed in terms of the nature of the microscopic degree of freedom, be that the magnetic moments (in ferromagnet/paramagnet), or electric dipoles (in ferroelectric/paraelectric), or octahedral degrees of freedom (e.g., tilting and rotations) [1–5]. X-ray diffraction (XRD) measurements [6] on such cubic

Initially, in this approach, the disorder in the para-phases was treated by "structural approximants" avoiding molecular dynamics (MD). Notable examples include the "Virtual Crystal Approximation" (VCA) [49] and "Coherent Potential Approximation" (CPA) [50]. These approaches offer an effective configuration that could be used as input to standard electronic structure theory and capture some aspects of disorder. Whereas such models are ubiquitous for positionally disordered alloys, they are not gen-

the distortions related to different Goldschmidt factor and band-edge states. In this paper, we mainly focus on the semiconductor oxide ABO_3 ($A = \text{Ba, Sr, Ca, Pb}$; $B = \text{Ti, Zr}$), and halide $CsBX_3$ ($B = \text{Ge, Sn, Pb}$; $X = \text{F, Br, I}$), $KPbI_3$ and $RbPbI_3$, and show three

ful “structural approximants” for describing the electronic structure of realistic cubic perovskites before thermal agitation sets in. The thermally induced disorder is then added at the DFT molec-

gap by taking ATiO_3 ($A^+ = \text{Ca, Sr, Ba}$) and CsBI_3 ($B^{2+} = \text{Pb, Sn}$) as examples.

The multi-mode distortions can lower the energy more than the single-mode distortions because of a few reasons. First, instead of having a single-mode with a large, uniform tilting angle and/or displacement throughout the lattice, it is sometimes energetically advantageous to have a few modes covering a range of tilting angles or displacements. Given the similar energy lowering for a single-mode distortion with a large tilting angle and a few modes with small tilting angles, we anticipate that modes such as $a^-a^-a^-$, $a^0a^0b^-$ and $a^0b^-b^-$ modes in SrTiO_3 , $a^0a^0b^-$ and $a^0a^0b^+$ modes in CsPbI_3 , as well as $a^-a^-a^-$, $a^0b^-b^-$, and $a^-a^-a^+$ modes in CaTiO_3 would coexist. The similar energy lowering of different single-mode distortions might lead to a mixture of different tilting modes with energy lowering. Indeed, as depicted in Fig. 1, the mixture mode $(a^0a^0b^-)_1^2 (a^0a^0b^+)_2^3 (a^0a^0b^-)_3^4$ in $4 \times 4 \times 4$ supercell of the cubic SrTiO_3 has slightly

lower energy (by 1 meV/f.u.) than the $2 \times 2 \times 2$ supercell with the single a

TABLE 2

The DFT energy lowering ΔE_{M-P} due to multi-mode distortions in polymorphous structures compared with the energy of the nominal cubic (Pm-3m) structure was calculated by using the PBEsol functional. These polymorphous structures with multi-mode distortions were obtained by minimization of internal forces of the nudged, cubically shaped 4

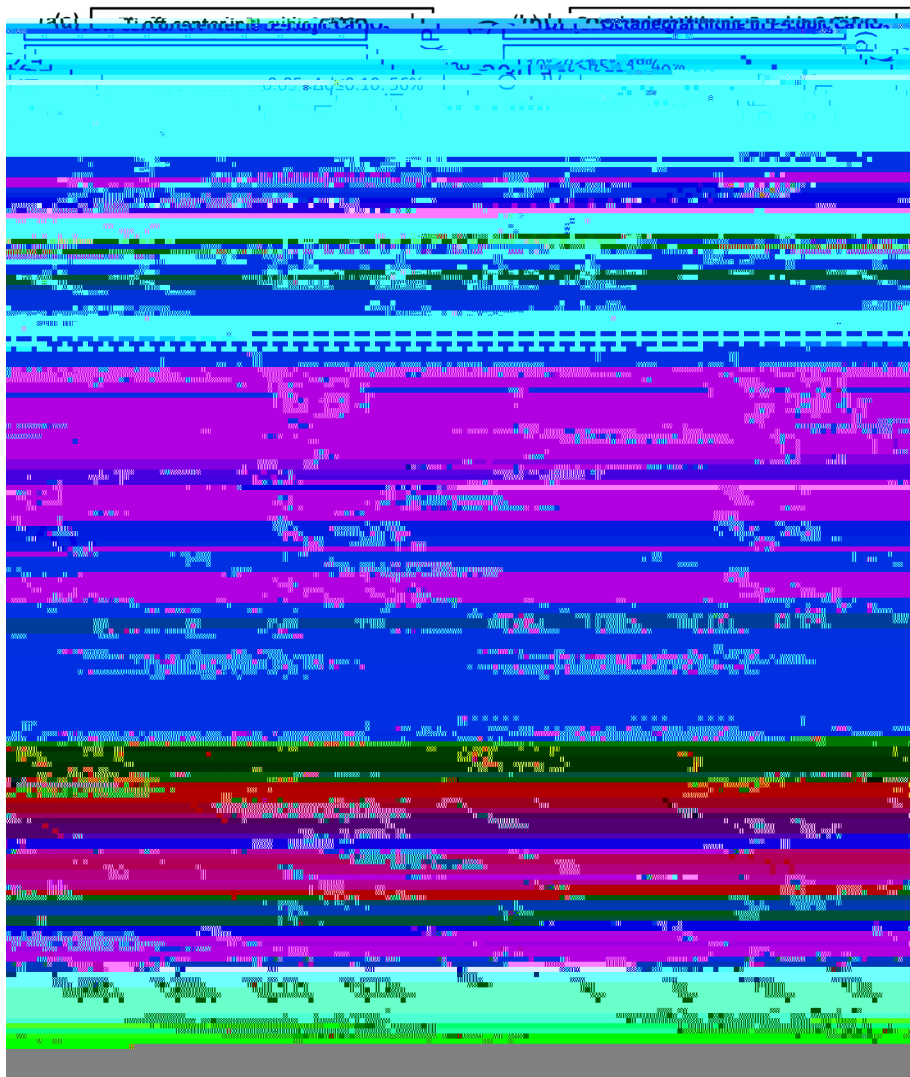


FIGURE 3

$\Delta E_{M-P} = E_{M-P} - E_{Pm-3m}$. The energy lowering ΔE_{M-P} is calculated as the difference between the energy of the distorted structure E_{M-P} and the energy of the nominal cubic structure E_{Pm-3m} . The energy is calculated using the PBEsol functional. The distorted structures are obtained by minimizing the internal forces of the nudged, cubically shaped 4

atomic distances and short-range order. This information, not addressed in the present paper, awaits to be mined in the form of SRO parameters and PDF data as reported in Ref. [28]. The PDF is a local probe that reflects the distribution of atom–atom distances, thus a good way to determine the local atomic configurations and distortion of local motifs within the system. As already noted, fitting the diffraction data in the Rietveld process to a single formula cubic (Pm-3m) cell [72] can miss the existence of intrinsic DOWPs that evidently lead to energy lowering (Fig. 1

5p at VBM and Pb-6p – I-5p at CBM as illustrated in [Fig. 8d](#)). We find that the octahedral rotation in CaTiO_3

To analyze the relationship between the direct gap component and the rotation DOWPs, Fig. 9b shows several cubic SrTiO₃ with frozen-in a⁰b⁻b⁻ mode with a rotation angle of 0°, 2.5°, and 5°. The increase in rotation amplitude causes the VBM spectral intensity at Γ to increase, but VBM spectral intensity at R diminishes. These trends signal the buildup of a significant direct band gap component in cubic SrTiO₃ due to tilting DOWPs.

D. Effects of single-mode and multi-mode static non-thermal deformations on band gaps

Fig. 10 summarizes for several cubic ABX₃ compounds (i) the minimal band gap from monomorphous (Pm-3m) cell (shown in

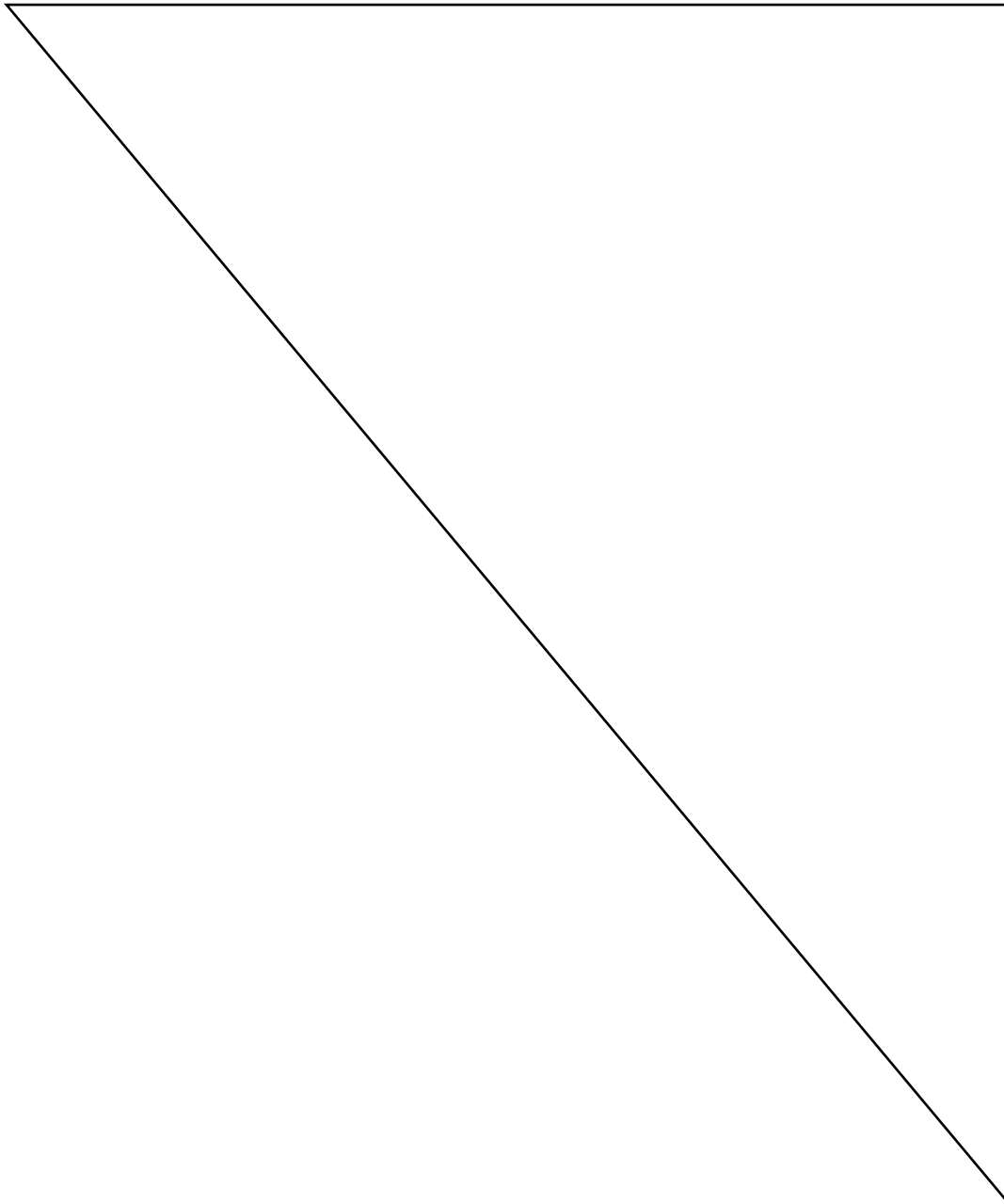
blue), (ii) the gap resulting from allowing single-mode DOWPs

multi-mode DOWPs in polymorphous network show much larger blueshift values from 0.11 eV for BaTiO₃ to 0.55 eV for CsSnI₃. Local symmetry breaking, either single-mode or multi-mode DOWPs, can lead to significant band gap blueshift.

Effect of temperature-induced distortion in molecular dynamics on band gaps

A. DFT molecular dynamics: Temperature-enhanced deformations in CaTiO₃ and SrTiO₃

The free energy of the vibrating lattice $F = U_0 - TS$ at finite temperature can be studied using MD simulations. As the tem-



mally enhanced atomic displacements at finite temperatures are consistent with enlarged Li displacements (rather than diminished displacements) as temperature increase in paraelectric LiNbO₃ [39].

B. The effects on band gap shift due to thermal distortion in oxide perovskites

The enhanced thermal motions revealed by the AIMD simulations result in significant band gap changes. For instance, the

averaged band gap (expressed as $\sum_{i=1}^N E_g(S_i)/N$ of individual configuration S_i along the thermodynamic equilibrium trajectory $E_g(S_i)$ refers to the allowed and forbidden band gap of S_i) and S_i) for cubic CaTiO₃ and SrTiO₃ are shown in Table 1. The band gap redshift due to thermal motions at 2000 K in cubic CaTiO₃ is 1.15 eV with respect to polymorphous structure, and 0.77 eV with respect to the nominal cubic structure. Similarly, in cubic SrTiO₃, the corresponding band gap redshifts are 0.72 eV and 0.49 eV, respectively, at 1400 K. Evidently, thermal motions in cubic CaTiO₃ and SrTiO₃ lead to significantly band gap redshift

Table 1 provides both a preview and a succinct summary of the main differences between the effects of static non-thermal vs. dynamic thermal displacements on band gaps for oxide perovskites.

For oxide perovskites: Different from nominal cubic SrTiO_3 and CaTiO_3 with p-like VBM and d-like CBM, the “correlated” Mott insulators having

at high temperature ($>T_c$) compared with band gap at $T = 0$ (monomorphous structure).

- [14] R.A. Evarestov, V.P. Smirnov, D.E. Usvyat, *Solid State Commun.* 127 (2003) 423–426.
- [15] A.R. Benrekia et al., *Physica B* 407 (2012) 2632–2636.
- [16]